PHYSICAL REVIEW B **85**, 115208 (2012)

Lattice thermal conductivity of $(\mathrm{Bi}_{1-x}\mathrm{Sb}_x)_2\mathrm{Te}_3$ alloys with embedded nanoparticles

N. A. Katcho,[1] N. Mingo,[1] and D. A. Broido[2]
[1] *LITEN, CEA-Grenoble, 17 rue des Martyrs, 38054 Grenoble Cedex 9, France*
[2] *Department of Physics, Boston College, Chestnut Hill, Massachusetts 02467, USA*

(Received 24 November 2011; revised manuscript received 30 January 2012; published 30 March 2012)

The lattice thermal conductivity of $(\mathrm{Bi}_{1-x}\mathrm{Sb}_x)_2\mathrm{Te}_3$ alloys, with and without spherical nanoparticle inclusions, has been computed using the Boltzmann transport equation with classical interatomic potentials within the relaxation time approximation. The experimental thermal conductivity of the pure alloys is fairly well reproduced as a function of concentration. We establish upper and lower limits for the thermal conductivities that could be obtained via seamlessly embedded spherical nanoparticles as a function of their size, density, and volume fraction. Large reductions in thermal conductivities (40–50%) can only be achieved with small nanoparticles with diameters below 10 nm.

DOI: 10.1103/PhysRevB.85.115208   PACS number(s): 66.70.Df, 63.50.Gh

I. INTRODUCTION

Alloys (or solid solutions) of BiSbTeSn are currently the best compounds for commercial room temperature thermoelectric energy conversion. Very recently, it has been possible to increase the dimensionless thermoelectric figure of merit[1] ZT of bulk $(\mathrm{Bi}_{1-x}\mathrm{Sb}_x)_2\mathrm{Te}_3$ alloys from its long standing value of 1, up to $ZT = 1.4$, via sintering of nanosized powders.[2,3] This increase is mainly due to a large reduction of the lattice thermal conductivity κ_L induced by enhanced phonon scattering at grain boundaries, defects, nanodots, and precipitates generated during the synthesis process.

Despite its importance, κ_L of $(\mathrm{Bi}_{1-x}\mathrm{Sb}_x)_2\mathrm{Te}_3$ alloys has not been theoretically explored in detail because of the complexity of this system, constituted by heavy elements bonded by partially covalent bonds and arranged in a complicated crystal structure.[4] Only recently interatomic potentials suitable to describe anharmonic effects in $\mathrm{Bi}_2\mathrm{Te}_3$ have been developed.[5,6] They have been used to investigate, by molecular dynamics (MD) simulations, the mechanical and/or transport properties of bulk $\mathrm{Bi}_2\mathrm{Te}_3$,[5–7] $\mathrm{Bi}_2\mathrm{Te}_3$ nanowires,[8,9] and $\mathrm{Bi}_2\mathrm{Te}_3$ nanofilms.[10] The question of whether κ_L of $(\mathrm{Bi}_{1-x}\mathrm{Sb}_x)_2\mathrm{Te}_3$ alloys can also be well described for any arbitrary concentration x is therefore a relevant one. Here we show that with a suitable rescaling of the interatomic potentials developed initially for $\mathrm{Bi}_2\mathrm{Te}_3$, it is possible to solve the Boltzmann transport equation (BTE) for phonons, with dispersions and alloy scattering rates calculated from these rescaled potentials, and derive thermal conductivities for $(\mathrm{Bi}_{1-x}\mathrm{Sb}_x)_2\mathrm{Te}_3$ alloys which are in fair agreement with experimental results at any concentration.

A second, more pressing question is to what extent the presence of nanoinclusions can affect the thermal conductivity of these alloys. The fundamental role of the nanoinclusions in decreasing the thermal conductivity below that of the alloy has been established previously.[11] Such a nanoparticle-embedded-in-alloy thermoelectric (NEAT) approach[12] has been experimentally demonstrated for ErAs nanoparticles in a InGaAs matrix[13] and theoretically investigated for silicide nanoinclusions in a SiGe matrix.[14–16] At present, $(\mathrm{Bi}_{1-x}\mathrm{Sb}_x)_2\mathrm{Te}_3$ alloys with embedded nanoparticles and high ZT values have been experimentally reported,[2,3,17] but the decrease of κ_L due to the presence of nanoparticles has not been quantified. Our calculations show that, using nanoparticle volume fractions below 3% in an otherwise defect-free matrix, one does not expect reductions beyond 40–50%. Such decrease can only be achieved for nanoparticle diameters not exceeding 10 nm.

The following sections contain a description of the theoretical approach (II) and a discussion of the results and their implications (III), followed by a summary and conclusions (IV).

II. THEORY

This section gives details on the computation of the lattice thermal conductivity, the calculation of the alloy scattering rates, and the interatomic potentials.

A. Lattice thermal conductivity

In the relaxation time approximation (RTA) the thermal conductivity κ_L is given by an integral over frequency ω as[16]

$$\kappa_L(T) = \frac{1}{k_B T^2}\int_0^\infty n_0(\omega)[n_0(\omega)+1](\hbar\omega)^2\Sigma^{\mathrm{ph}}(\omega)d\omega \quad (1)$$

with $n_0(\omega) = [\exp(\hbar\omega/k_B T) - 1]^{-1}$ being the equilibrium Bose distribution function and

$$\Sigma^{\mathrm{ph}}(\omega) = \frac{1}{8\pi^3}\sum_\alpha \int_{\mathrm{BZ}} \tau_{\alpha,\mathbf{q}}\left(v^z_{\alpha,\mathbf{q}}\right)^2 \delta(\omega - \omega_{\alpha,\mathbf{q}})d\mathbf{q}. \quad (2)$$

Here the integral runs over the Brillouin zone. $\omega_{\alpha,\mathbf{q}}$ represents the angular frequency of the normal mode with wave vector $\mathbf{q}$ and branch index α, $\tau_{\alpha,\mathbf{q}}$ is the phonon relaxation time, and $v^z_{\alpha,\mathbf{q}}$ is the component of the phonon group velocity along the direction of the thermal gradient (z in the above expression). The normal vibrational modes of the system are obtained by solving the classical equations of motion in the harmonic approximation for each $\mathbf{q}$ point used in the sampling of the Brillouin zone. These equations take the form of an eigenvalue problem:[19]

$$\omega^2_\lambda|\lambda\rangle = \mathbf{D}(\mathbf{q})|\lambda\rangle, \quad (3)$$

where we label the phonon $(\alpha,\mathbf{q})$ by the symbol λ. $\mathbf{D}(\mathbf{q})$ is the dynamical matrix which contains the force constants (second derivatives of the interatomic potential) and $|\lambda\rangle$ is the eigenvector that specifies the displacement of each atom of the unit cell for the corresponding phonon mode. When the system is polar, as is the case of $(\mathrm{Bi}_{1-x}\mathrm{Sb}_x)_2\mathrm{Te}_3$ alloys, $\mathbf{D}(\mathbf{q})$ has a long-range contribution due to the electrostatic interactions. The technical details to deal with these long-range interactions can be found in Gonze *et al.*.[20]

Once the $\omega_{\alpha,\mathbf{q}}$ and $|\lambda\rangle$ are obtained through the diagonalization of the dynamical matrix, the group velocities $\mathbf{v}_\lambda$ can be calculated:

$$\mathbf{v}_\lambda = \nabla_{\mathbf{q}}\omega_\lambda. \tag{4}$$

Application of the Hellmann-Feynman theorem[21] to Eq. (3) leads to an expression equivalent to Eq. (4) but more suitable for its practical implementation:

$$\mathbf{v}_\lambda = \frac{1}{2\omega_\lambda}\sum_i\sum_j \langle\lambda|i\rangle\nabla_{\mathbf{q}}D_{ij}(\mathbf{q})\langle j|\lambda\rangle, \tag{5}$$

where the indexes i and j run over all degrees of freedom of the unit cell.

B. Scattering rates

In general, the τ's in Eq. (1) can be calculated from iteratively solving the BTE, using the 2- and 3-phonon scattering probabilities obtained from the interatomic potential.[22] A much simpler approach is to employ approximated analytical expressions for the τ's,[18] which introduces adjustable parameters. For the alloys considered here, we will show that one needs a total of three experimentally adjustable parameters. Two of them, related to the anharmonicity, require the knowledge of κ_L for pure $\mathrm{Bi}_2\mathrm{Te}_3$ and for pure $\mathrm{Sb}_2\mathrm{Te}_3$. The third one is needed to account for bond disorder effects. On the other hand, the alloy scattering due to mass disorder and the nanoparticle scattering contributions are calculated directly from the atomistically computed phonon structure, without any adjustable parameter, as we explain below.

The different scattering contributions are combined following Mathiessen's rule to yield the total scattering rate, $\tau^{-1}(\lambda)$, as a sum of anharmonic (a), alloy disorder (d), and nanoparticle (np) scattering contributions:

$$\tau^{-1}(\lambda) = \tau_a^{-1}(\omega_\lambda) + \tau_d^{-1}(\lambda) + \tau_{\mathrm{np}}^{-1}(\lambda). \tag{6}$$

At temperatures near or above the Debye temperature, the anharmonic scattering rate is reasonably well described by a dependence[23]

$$\tau_a^{-1}(\omega) = BT\omega^2. \tag{7}$$

The B parameter is individually adjusted for each of the two pure phases, $\mathrm{Bi}_2\mathrm{Te}_3$ and $\mathrm{Sb}_2\mathrm{Te}_3$, by fitting their experimental bulk crystal thermal conductivities. For a $(\mathrm{Bi}_{1-x}\mathrm{Sb}_x)_2\mathrm{Te}_3$ alloy, we take the weighted average parameters: $B = (1-x)B_{\mathrm{Bi}_2\mathrm{Te}_3} + xB_{\mathrm{Sb}_2\mathrm{Te}_3}$.

The scattering due to the disordered arrangement of Sb and Bi atoms in the alloy is computed within an effective medium approach originally employed by Abeles.[24] In this approach the alloy is assumed to be a random mixture of atoms. The disordered lattice is replaced by an ordered virtual crystal with properties averaged between those of the pure components. An atom of the virtual crystal is then replaced by an atom of the alloy, which acts as a virtual impurity and scatters phonons. The impurity scattering is due to mass and bond disorder of the random alloy. In the Born approximation, the scattering rate is given by[16]

$$\tau_d^{-1}(\lambda) = f\frac{\Omega}{V_{\mathrm{imp}}}\frac{\pi}{2}\left[\left(\frac{\Delta M}{M}\right)^2 + \epsilon\left(\frac{\Delta r}{r}\right)^2\right]\omega_\lambda^2 \times \sum_{i,j}\langle\lambda|i\rangle\langle i|\hat{\rho}_{\mathrm{ph}}|j\rangle\langle j|\lambda\rangle, \tag{8}$$

where f represents the volume fraction of impurities, V_{imp} is the volume of the impurity, Ω is the volume into which the phonon eigenstates $|\lambda\rangle$ are normalized, M and r are the host atomic mass and radius, respectively, and $\Delta M = M_i - M$ and $\Delta r = r_i - r$ are the difference between the impurity and host atomic masses and radius. ϵ is a phenomenological, adjustable parameter, introduced by Abeles[24] to account for bond disorder. The local indexes i and j run through the three atomic degrees of freedom of the impurity, and $\langle i|\hat{\rho}_{\mathrm{ph}}|j\rangle$ is the phonon density of states matrix. In the effective medium approach, M represents the atomic mass in the virtual crystal, and the total impurity scattering rate is obtained by adding the scattering rates of each virtual impurity (Bi and Sb in our case). For a $(\mathrm{Bi}_{1-x}\mathrm{Sb}_x)_2\mathrm{Te}_3$ alloy, taking as reference the rhombohedral unit cell (5 atoms per unit cell), $M = (1-x)M_{\mathrm{Bi}} + xM_{\mathrm{Sb}}$, $\Delta M_{\mathrm{Bi}} = x(M_{\mathrm{Bi}} - M_{\mathrm{Sb}})$, $\Delta M_{\mathrm{Sb}} = (1-x)(M_{\mathrm{Sb}} - M_{\mathrm{Bi}})$, $V_i = [(1-x)V_{\mathrm{Bi}_2\mathrm{Te}_3} + xV_{\mathrm{Sb}_2\mathrm{Te}_3}]/5$, where $V_{\mathrm{Bi}_2\mathrm{Te}_3}$ and $V_{\mathrm{Sb}_2\mathrm{Te}_3}$ are the corresponding unit cell volumes. We have taken the covalent radius[25] for r_i ($r_{\mathrm{Bi}} = 0.148$ nm, $r_{\mathrm{Sb}} = 0.139$ nm) and r was calculated in the same way as M. Approximating the volume fraction f by the molar fraction, then $f_{\mathrm{Sb}} = \frac{2x}{5}$, $f_{\mathrm{Bi}} = \frac{(2-2x)}{5}$. The density of states matrix should reflect the point symmetry of the virtual crystal lattice site where the impurity is located. In our case, the point symmetry is $3m$, which makes the matrix diagonal with $\rho_{\mathrm{ph},11} = \rho_{\mathrm{ph},22} \neq \rho_{\mathrm{ph},33}$.

Even in the effective medium approach, the bond disorder is not rigorously described by Eq. (8). However, a suitable choice of the ϵ parameter makes it possible to derive in a simple way thermal conductivities in good agreement with experiment in the entire range of compositions. On the other hand, this simplified model for the bond disorder has no influence in the study of the embedded nanoparticles since, as we will show, nanoparticles mainly scatter the low-frequency phonons for which the anharmonic scattering is much stronger than the alloy one.

The nanoparticle scattering contribution is computed using an interpolation between the long- and short-wavelength scattering regimes:[16]

$$\tau_{\mathrm{np}}^{-1} = \left(\frac{1}{\tau_s^{-1}} + \frac{1}{\tau_l^{-1}}\right)^{-1} = v\left(\sigma_s^{-1} + \sigma_l^{-1}\right)^{-1}\rho. \tag{9}$$

s and l stand for short and long wavelength, respectively, v is the phonon velocity, ρ is the density of nanoparticles, and σ_s and σ_l are the corresponding scattering cross sections. Assuming spherical nanoparticles of radius R, noting that σ_s is twice the geometrical cross section[11] and that ρ can be related to the volume fraction of nanoparticles f and the volume of an individual nanoparticle V_{np} through $\rho = f/V_{\mathrm{np}}$, the short-wavelength limit is given by

$$\tau_s^{-1} = v2\pi R^2\frac{f}{V_{\mathrm{np}}}. \tag{10}$$

The long-wavelength limit for a nanoparticle constituted by N cells of the virtual crystal is given, in the Born approximation, by a generalization of Eq. (8) for the disorder scattering:[16]

$$\begin{aligned}\tau_l^{-1}(\lambda) &= f N \frac{\pi}{2}\omega_\lambda^2 D_\lambda,\\ D_\lambda &= \sum_{\alpha'} \int \left| \sum_i \left(\frac{\Delta M_i}{M}\right) \langle\lambda|i\rangle\langle i|\lambda'\rangle \right|^2\\ &\quad \times |S_{\Delta\mathbf{q}}|^2 \delta(\omega_{\lambda'}-\omega_\lambda)\frac{d\mathbf{q}'}{V_{\mathrm{BZ}}}.\end{aligned} \tag{11}$$

Now the index i runs through all degrees of freedom of the unit cell, $\Delta\mathbf{q} = q - q'$, and $S_{\Delta\mathbf{q}} = \frac{1}{N}\sum_T e^{\Delta\mathbf{q}\cdot\mathbf{T}}$ is the structure factor for the nanoparticle, where $\mathbf{T}$ represents the lattice translation vector for each cell that belongs to the nanoparticle. However, Eq. (11) is somewhat incomplete as it neglects the scattering due to the differences between the nanoparticle and matrix force constants and/or crystal structure, and also to the strain field that could be originated by the lattice mismatch, if any.[26] Therefore, taking into account only the scattering due to the mass difference between the matrix and the nanoparticle ensures that the calculated thermal conductivity constitutes an upper bound. A lower bound can also be estimated. From Eq. (9) it can be seen that the actual scattering cross section of the nanoparticle cannot be larger than σ_s and σ_l at any frequency. While at high frequencies $\sigma_l \gg \sigma_s$ and $\sigma_{\mathrm{np}} \sim \sigma_s$, at low frequencies $\sigma_l \ll \sigma_s$ and $\sigma_{\mathrm{np}} \sim \sigma_l$. The transition region between both regimes is determined by the density difference between the matrix and the nanoparticle, $|\Delta\rho|$. As $|\Delta\rho|$ increases, σ_l becomes larger, the transition takes place at lower frequencies, and σ_s dominates over a wider frequency range, decreasing the lattice thermal conductivity. The lower bound, i.e., the largest possible reduction of the thermal conductivity, is achieved when $\sigma_{\mathrm{np}} = \sigma_s$ for all frequencies. This lower bound corresponds to $\Delta\rho = \infty$, the limit of infinite mass at which the nanoparticle is completely rigid and can not transmit any lattice wave.

C. $(\mathrm{Bi}_{1-x}\mathrm{Sb}_x)_2\mathrm{Te}_3$ interatomic potentials and phonon density of states

An interatomic potential to calculate the lattice thermal conductivity of $\mathrm{Bi}_2\mathrm{Te}_3$ was developed by Huang and Kaviany[5] (henceforth the HK potential) by fitting the energy surface from *ab initio* calculations. It consists of a short-range interaction described by two- and three-body terms, and a long-range interaction (Coulombic terms) that is computed with the Ewald method.[27] Due to the complicated three-body term, Qiu and Ruan[6] modified the short-range part of the HK potential and developed a simpler expression based only on two-body terms (henceforth the QR potential). Both potentials reproduce well the experimental dispersion of acoustic-phonon modes but not the dispersion of the optical ones. This is probably due to the rigid-ion model that neglects the high polarizability of Bi and Te atoms. As the phonon transport is dominated by the acoustic-phonon modes, the lattice thermal conductivity predicted by both potentials is in good agreement with the available experimental data.

On the other hand, there has not been a similar theoretical work on the $\mathrm{Sb}_2\mathrm{Te}_3$ system and to the best of our knowledge no interatomic potential suitable to study the phonon transport properties of this system has been developed. However $\mathrm{Bi}_2\mathrm{Te}_3$ and $\mathrm{Sb}_2\mathrm{Te}_3$ are closely related materials whose atoms are arranged in the same crystalline structure, and due to their chemical similarity they can be combined in a solid solution $(\mathrm{Bi}_{1-x}\mathrm{Sb}_x)_2\mathrm{Te}_3$ for any composition. Then one should expect that the functional form of the $\mathrm{Bi}_2\mathrm{Te}_3$ interatomic potentials should be suitable also to describe the bonding in $\mathrm{Sb}_2\mathrm{Te}_3$ and its alloys.

The dispersion of the acoustic-phonon modes is almost linear, the slope depending on the elastic constants of the material. This suggests that with a suitable rescaling of the $\mathrm{Bi}_2\mathrm{Te}_3$ interatomic potential, for any alloy composition the low-frequency region of the phonon spectrum and then the lattice thermal conductivity could be well accounted for. Therefore the question is how to determine the rescaling factor for a given composition x. As we explain below, this rescaling factor can be inferred from the analysis of the experimental phonon density of states (PDOS).

The generalized PDOS of $\mathrm{Bi}_2\mathrm{Te}_3$, $(\mathrm{Bi}_{0.5}\mathrm{Sb}_{0.5})_2\mathrm{Te}_3$, and $\mathrm{Sb}_2\mathrm{Te}_3$ has been measured by inelastic neutron scattering.[28] At higher frequencies the main peak of the PDOS, $G(\nu)$, does not shift, which indicates that the corresponding lattice modes are mainly due to the motion of Te atoms. At the lower frequencies which are relevant to the thermal transport ($\nu < 2$ THz) the group V element strongly influences $G(\nu)$, as is expected since the low-frequency vibrational modes consist of the motion of all the atoms of the unit cell. Taking as a reference the PDOS of $\mathrm{Bi}_2\mathrm{Te}_3$, the corresponding low-frequency PDOSs of $(\mathrm{Bi}_{0.5}\mathrm{Sb}_{0.5})_2\mathrm{Te}_3$ and $\mathrm{Sb}_2\mathrm{Te}_3$ are shifted to higher frequencies by a factor of 1.19 and 1.43, respectively. If the shift were only due to the change in mass, the previous factor should be given by $\sqrt{M_{\mathrm{Bi}_2\mathrm{Te}_3}/M_{(\mathrm{Bi}_{1-x}\mathrm{Sb}_x)_2\mathrm{Te}_3}}$, which takes the values 1.06 and 1.13 for the equimolar and pure antimony alloys, respectively. Then it is clear that the observed shifts at low frequencies cannot be accounted for by considering only the mass ratio, but the change in force constants should be also taken into account. Therefore, to calculate the phonon modes of the $(\mathrm{Bi}_{1-x}\mathrm{Sb}_x)_2\mathrm{Te}_3$ alloys, one can use the following procedure. Starting with the potential for $\mathrm{Bi}_2\mathrm{Te}_3$, one replaces the Bi mass by $(1-x)M_{\mathrm{Bi}} + xM_{\mathrm{Sb}}$. This substitution accounts for the mass shift. To reproduce the experimental observed shift, the force constants are rescaled by the square of the empirical factor $1.19/1.06$ ($x = 0.5$) and $1.43/1.13$ ($x = 1.0$). For other values of x, one performs a quadratic interpolation. It is important to note that this rescaling only provides accurate results for the low-frequency region of the PDOS ($\nu < 2$ THz).

III. RESULTS

The RTA described in Sec. II constitutes a semiempirical approach that requires the knowledge of the experimental values of κ_L for the pure components of the alloy in order to set the B parameter of Eq. (7). Although MD simulations[5,6] have shown that the QR and HK potentials respectively underestimate and overestimate the κ_L of $\mathrm{Bi}_2\mathrm{Te}_3$ somewhat, when these potentials are used in the RTA with their corresponding B values we have not observed any significant differences in the κ_L calculated for the alloys. Due to the greater simplicity of the QR potential, we present the results obtained with it.

The PDOS and κ_L have been computed using the tetrahedron method[29] to integrate Eq. (2). A grid of 6370 **q** points belonging to the irreducible Brillouin zone was used. The adjustable parameter B was set by fitting the experimental data. κ has been measured as a function of composition by several authors.[30–33] In all cases κ was measured along the (111) plane. There are large differences between the different data sets, which are mainly attributed to the choice of the Lorenz number for the calculation of the electronic component of κ. For Bi_2Te_3 we have set $\kappa_L = 1.7$ W m^{-1} K^{-1}, in close agreement with the measurements of Birkholz,[31] Satterthwaite,[34] and Ismaiylova.[35] On the other hand, Sb_2Te_3 has not been as extensively studied as Bi_2Te_3. In Fig. 2 very large discrepancies can be seen between different measurements for Sb_2Te_3. Using the Lorenz number 2.1×10^{-8} reported by Stordeur and Simon,[36] the κ_L derived from recent measurements of the total thermal conductivity[37,38] is approximately 1.8 W m^{-1} K^{-1}, close to the value of 1.65 reported by Goldsmid.[30] We have set the same κ_L value for Sb_2Te_3 which leaves the B parameter invariant. The ϵ parameter has been set by fitting κ_L for $x = 0.75$.

This is the optimum composition for thermoelectric applications, and the one we have used to investigate the NEAT approach. The fitted values are $B_{\mathrm{Bi_2Te_3}} = B_{\mathrm{Sb_2Te_3}} = 7.6 \times 10^{-18}$ s/K, $\epsilon = 150$. The fitted B is of the same order of magnitude as the B predicted by Eq. (13) of the work of Klemens,[23] which relates B with κ_L ($\sim$1.7 W m^{-1} K^{-1}), the sound velocity ($\sim$2000 m/s),[5,37] and the Debye temperature ($\sim$160 K).[37] It is also of the same order as the one reported for Sb_2Te_3 by Yang *et al.*.[39] The fitted ϵ makes the contribution of bond disorder of the same order as the mass disorder one. This can be understood comparing the relative changes in mass ($\Delta M/M$) and force constants ($\Delta K/K$), the latter one derived from the rescaling factors (see Sec. II C). For $x = 0.5$, $\Delta M/M \sim 0.26$, $\Delta K/K \sim 0.23$, which are almost equal.

The experimental generalized PDOS and the corresponding theoretical PDOS are shown in Fig. 1. For Bi_2Te_3 the PDOS derived from MD[6] is also shown. The finite simulation time of the MD broadens the spectrum, but there is a very good agreement between our calculated PDOS and that of Qiu and Ruan[6] regarding the position of the spectrum maxima, the width of the gap, and the cutoff frequency. The generalized PDOSs shown in Fig. 1 are weighted representations of the true PDOSs, with the contribution of each atom weighted by its neutron scattering length. Then a direct comparison with the theoretical PDOS should not be attempted, but only the position of peaks should be compared. The acoustic PDOS of Bi_2Te_3 ($0 \sim 1.6$ THz) correlates well with the position of the experimental peaks. This is the contribution to the total PDOS that needs to be well described since, at 300 K, the heat transport is largely dominated by these phonons. Our calculations predict that the acoustic phonons carry more than 90% of the heat. The contribution derived from MD simulations is of similar order.[5] The agreement holds also for $(Bi_{0.5}Sb_{0.5})_2Te_3$ and Sb_2Te_3, as expected, since the rescaling factor was derived from the observed experimental shifts. Regarding the optical phonon modes, we can see that the gap predicted by the QR potential for Bi_2Te_3 is absent in the experiment, overestimating the frequencies of the optical modes. For $(Bi_{0.5}Sb_{0.5})_2Te_3$ and Sb_2Te_3 the agreement is even worse since our rescaling procedure is not longer valid for the high-frequency region of the phonon spectrum, but this limitation does not influence so much the calculated value of κ_L since anharmonic scattering is described through the parameter B, which is adjusted to match the measured κ_L value of the matrix material.

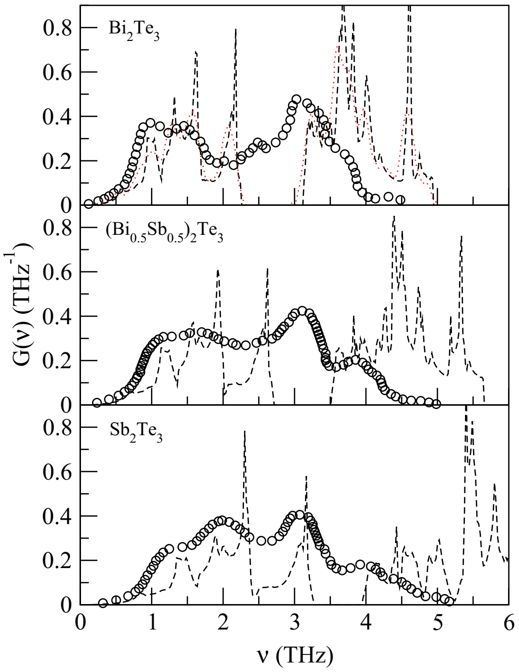

FIG. 1. (Color online) Circles: Generalized PDOS measured by inelastic neutron scattering (Ref. 28). Dashed lines: Theoretical PDOS derived from the diagonalization of the dynamical matrix. Dotted line: Theoretical PDOS derived from MD (Ref. 6).

The predicted κ_L parallel to the (111) plane, together with the experimental conductivities measured by Goldsmid,[30] Birkholz,[31] and Rosi[32] along this plane, are shown in Fig. 2 as a function of composition, x. The recent measurement of Poudel *et al.*[2] is also shown. The calculated κ_L curve goes through the experimental data sets of Goldsmid[30] and Rosi,[32] with discrepancies no larger than 15% on the Bi_2Te_3-rich side. The three experimental data sets show an asymmetric shape, with the minimum located at $x \sim 0.75$. The calculated curve is nearly symmetric, with the minimum close to the equimolar composition. This is due to the limitation of the simplified bond disorder model we have used. Regarding the alloy's conductivity along the perpendicular direction, we have found experimental data only for pure Bi_2Te_3. The experimental ratio between conductivities along and perpendicular to the (111) plane is about 2.0.[40] The predicted value is 1.7, in good agreement with previous MD simulations.[5,6]

We now shall focus on the reduction of κ_L due to the presence of nanoparticles in the alloy matrix. Experimentally, high ZT values ($ZT \sim 1.4$) have been reported[2,3] for an alloy matrix with composition $(Bi_{0.25}Sb_{0.75})_2Te_3$, close to the minimum in Fig. 2. This is the composition we have chosen to calculate κ_L for a range of $\Delta\rho$ that covers the experimental one. To the best of our knowledge, bismuth

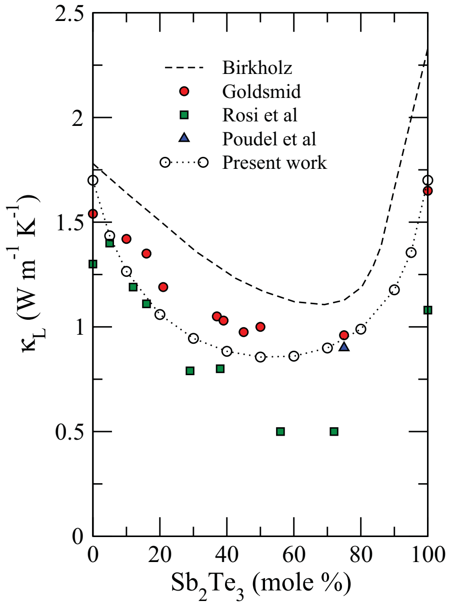

FIG. 2. (Color online) Predicted κ_L along the (111) plane at 300 K as a function of composition, compared with the experimental data of Birkholz (Ref. 31), Rosi *et al.* (Ref. 32), Goldsmid (Ref. 30), and Poudel *et al.* (Ref. 2).

telluride NEATs have been reported containing nanoinclusions of Te ($\Delta\rho/\rho \sim 8\%$, Ref. 2), Sb ($\Delta\rho/\rho \sim 1\%$, Ref. 3), ZnAlO ($\Delta\rho/\rho \sim 18\%$, Ref. 17), SiC ($\Delta\rho/\rho \sim 53\%$, Ref. 41), and also $(\mathrm{Bi}_{1-x}\mathrm{Sb}_x)_2\mathrm{Te}_3$ with x different from the alloy matrix composition ($\Delta\rho/\rho < 13\%$, Refs. 2 and 3). In Fig. 3 we show the calculated lattice thermal conductivities as a function of the diameter of the nanoparticles for a series of nanoparticle mass densities (symbols), for a 2% volume fraction. These curves represent an upper limit to the thermal conductivity (see Sec. II). The geometric (lower) limit obtained using Eq. (10) instead of Eq. (9) is also shown (solid line). The conductivities shown correspond to the effective conductivities of a polycrystalline material. We have obtained these conductivities using our calculated conductivities parallel and perpendicular to the (111) plane within an effective medium model.[42] There is a minimum thermal conductivity at an optimal nanoparticle size, which depends on the mass difference between the matrix and the nanoparticle. From Eqs. (10) and (11) it can be seen that, for a given volume fraction f, τ_l^{-1} increases with R while τ_s^{-1} decreases, which implies that κ_L decreases or increases with R depending on the scattering regime that dominates. The minimum is found at the transition region between both regimes. The inset of Fig. 3 shows that this minimum roughly varies as $\Delta\rho^{-1}$. The exact position of the minimum depends weakly on the volume fraction.

A significant reduction of the thermal conductivity is only achieved for quite small nanoparticle sizes ($\sim$10 nm) and large mass differences ($\Delta\rho/\rho \sim 50\%$). This situation is rather different from the one encountered for silicide nanoparticles embedded in a SiGe alloy matrix.[14,15] It was shown there that a 3.4% volume fraction results in much larger reductions of κ_L (more than four times below the alloy's thermal conductivity) than the ones shown by Fig. 3 for a 2% volume fraction. Furthermore the minimum for SiGe alloys is much wider than in the case of BiSbTe alloys, and large deviations in particle size still yield thermal conductivities nearly as low as the minimum. As we explain below, these strong differences are ultimately

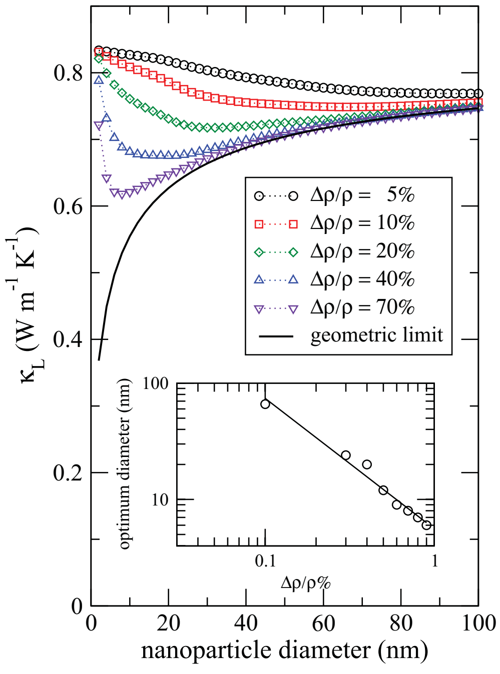

FIG. 3. (Color online) Thermal conductivity of $(\mathrm{Bi}_{0.25}\mathrm{Sb}_{0.75})_2\mathrm{Te}_3$ with 2% volume fraction of nanoparticles. Symbols: Upper limits for different $\Delta\rho$. Solid line: Lower limit (geometric scattering). The inset show the position of the minimum as a function of $\Delta\rho$. It roughly varies as $\Delta\rho^{-1}$.

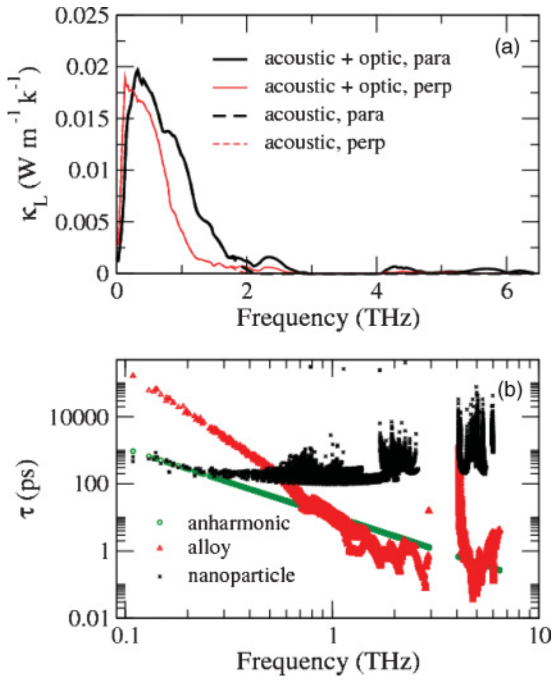

FIG. 4. (Color online) (a) Total and acoustic contributions to κ_L as a function of the phonon frequency for the alloy with $x = 0.75$. (b) Corresponding phonon lifetimes for anharmonic, alloy, and nanoparticle scattering for 2% volume fraction of nanoparticles, 10 nm nanoparticle diameter, and $\Delta\rho/\rho = 40\%$.

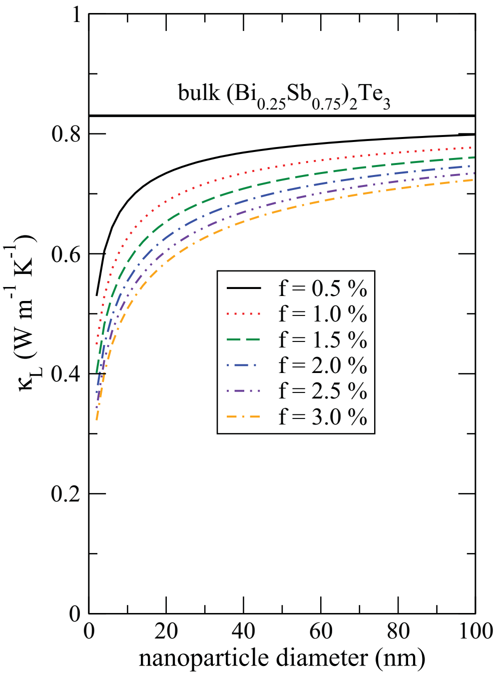

FIG. 5. (Color online) Lower limits for the thermal conductivity as a function of nanoparticle size, for a series of volume fractions. κ_L for the bulk alloy is also shown.

related to a relatively stronger anharmonicity than in the SiGe system. Figure 4(a) shows the total and acoustic contributions to κ_L for the alloy with $x = 0.75$. Acoustic phonons carry about the 90% of the total heat. In Fig. 4(b) we show the anharmonic, alloy, and nanoparticle phonon lifetimes, for a 2% volume fraction of 15 nm radius nanoparticles and $\Delta\rho/\rho = 40\%$. The effect of the embedded nanoparticles is small because at low frequencies the anharmonic and nanoparticle scattering are of the same order, which is a direct consequence of a stronger anharmonicity. Hence the fraction of heat-carrying phonons that are affected by the nanoparticles is reduced to the very lowest frequencies, as can be inferred from Fig. 4. Anharmonic scattering affects the scattering of all acoustic phonons, whereas alloy scattering becomes significant only for acoustic phonons with frequencies larger than 0.7 THz.

Finally, in Fig. 5 the geometric limit is shown for a series of nanoparticle volume fractions. The usefulness of this figure is twofold. On the one hand it predicts the κ_L reduction for nanoparticle diameters larger than 40 nm, for which the upper and lower limits coincide, as can be inferred from Fig. 3 ($\Delta\rho/\rho \geqslant 40\%$). In this case scattering is dominated by the geometric regime, and κ_L becomes independent of the chemical nature of the nanoparticle and depends only on its size and volume fraction. For a 3% volume fraction the decrease of the thermal conductivity is expected to be about 20% for 40 nm diameter nanoparticles. On the other hand, for small nanoparticles κ_L depends also on the chemical nature (composition and elastic constants) and the strain state of the nanoparticle. Although Fig. 4 can no longer be used to predict κ_L, it is still useful: For a given κ, the geometric limit sets a rough upper limit for the nanoparticle size. To achieve a reduction of about 40% ($\kappa_L \sim 0.5$ W m^{-1} K^{-1}), the nanoparticle diameter cannot exceed 10 nm for a 3% volume fraction. If significant stress is built around the nanoparticle, the effective diameter will be larger. If the volume fraction decreases, the nanoparticle should be even smaller. Experimentally, large κ_L reductions in nanograined bismuth antimony telluride alloys have previously been ascribed to the combined effects of nanoparticle and grain boundary scattering.[2,3] Our results above suggest that this experimental reduction is likely due to grain boundary scattering to a larger extent than to embedded nanoparticles.

IV. CONCLUSIONS

The current classical interatomic potentials developed for Bi_2Te_3, suitably rescaled, have been used to investigate the lattice thermal conductivity of $(Bi_{1-x}Sb_x)_2Te_3$ alloys. The computed lattice thermal conductivities are in fair agreement with experimental results in the entire range of compositions. The effect of embedded spherical nanoparticles has also been investigated. Reductions of thermal conductivity close to 50% can be achieved, but only under certain conditions regarding the size of the nanoparticle (diameter less than 10 nm) and its density difference compared to the embedded alloy ($\Delta\rho/\rho \sim 50\%$). These restrictions contrast with other systems such as silicides embedded in SiGe matrices where a very precise control of the size and chemical nature of the inclusion is not essential in order to produce the desired lowering of thermal conductivity. The existence of an optimal nanoparticle diameter is also predicted. Its origin is due to the transition between Rayleigh and geometrical scattering regimes, and it varies with density difference as $\Delta\rho^{-1}$. It becomes important when $\Delta\rho$ is large because of the narrowing of the minimum. When the differences in force constants are not negligible, the optimal sizes will be smaller than the ones predicted in the present work.

ACKNOWLEDGMENTS

We acknowledge support from the EU 7th Framework Programme through project NEAT. We thank D. A. Stewart and G. Bernard-Granger for helpful discussions.

---

[1] H. J. Goldsmid, *Thermoelectric Refrigeration* (Plenum, New York, 1964).

[2] B. Poudel, Q. Hao, Y. Ma, Y. Lan, A. Minnich, B. Yu, X. Yan, D. Wang, A. Muto, D. Vashaee, X. Chen, J. Liu, M. S. Dresselhaus, G. Chen, and Z. Ren, Science **320**, 634 (2008).

[3] Y. Ma, Q. Hao, B. Poudel, Y. Lan, B. Yu, D. Wang, G. Chen, and Z. Ren, Nano Lett. **8**, 2580 (2008).

[4] J. O. Jenkins, J. A. Rayne, and R. W. Ure, Phys. Rev. B **5**, 3171 (1972).

[5] B.-L. Huang and M. Kaviany, Phys. Rev. B **77**, 125209 (2008).

[6] B. Qiu and X. Ruan, Phys. Rev. B **80**, 165203 (2009).

[7] Y. Tong, F. J. Yi, L. S. Lui, P. C. Zhai, and Q. J. Zhang, Comput. Mater. Sci. **48**, 343 (2010).

[8] Y. Tong, F. J. Yi, L. S. Lui, and Q. J. Zhang, J. Electron. Mater. **39**, 1730 (2010).

[9] B. Qiu, L. Sun, and X. Ruan, Phys. Rev. B **83**, 035312 (2011).

[10] Y. Tong, F. J. Yi, L. S. Lui, P. C. Zhai, and Q. J. Zhang, Physica B **405**, 3190 (2010).

[11] W. Kim and A. Majumdar, J. Appl. Phys. **99**, 084306 (2006).

[12] M. Zebarjadi, K. Esfarjani, Z. Bian, and A. Shakouri, Nano Lett. **11**, 225 (2011).

[13] W. Kim, J. Zide, A. Gossard, D. Klenov, S. Stemmer, A. Shakouri, and A. Majumdar, Phys. Rev. Lett. **96**, 045901 (2006).

[14] N. Mingo, D. Hauser, N. P. Kobayashi, M. Plissonnier, and A. Shakouri, Nano Lett. **9**, 711 (2009).

[15] N. Mingo, D. Hauser, N. P. Kobayashi, M. Plissonnier, and A. Shakouri, Nano Lett. **10**, 2288 (2010).

[16] A. Kundu, N. Mingo, D. A. Broido, and D. A. Stewart, Phys. Rev. B **84**, 125426 (2011).

[17] T. Zhang, Q. Zhang, J. Jiang, Z. Xiong, J. Chen, Y. Zhang, W. Li, and G. Xu, Appl. Phys. Lett. **98**, 022104 (2011).

[18] N. Mingo, Phys. Rev. B **68**, 113308 (2003).

[19] M. T. Dove, *Introduction to Lattice Dynamics* (Cambridge University Press, Cambridge, 2005).

[20] X. Gonze and C. Lee, Phys. Rev. B **55**, 10355 (1997).

[21] R. P. Feynman, Phys. Rev. **56**, 340 (1939).

[22] D. A. Broido, M. Malorny, G. Birner, N. Mingo, and D. A. Stewart, Appl. Phys. Lett. **91**, 231922 (2007).

[23] P. G. Klemens, Phys. Rev. **119**, 507 (1960).

[24] B. Abeles, Phys. Rev. **131**, 1906 (1963).

[25] B. Cordero, V. Gómez, A. E. Platero-Prats, M. Revés, J. Echevarría, E. Cremades, F. Barragán, and S. Alvarez, Dalton Trans. **21**, 2832 (2008).

[26] P. G. Klemens, Proc. Phys. Soc. A **68**, 1113 (1955).

[27] P. P. Ewald, Ann. Phys. (Leipzig) **64**, 253 (1921).

[28] H. Rauh, R. Geick, H. Köhler, N. Nücker, and N. Lehner, J. Phys. C **14**, 2705 (1981).

[29] P. Lambin and J. P. Vigneron, Phys. Rev. B **29**, 3430 (1984).

[30] H. J. Goldsmid, J. Appl. Phys. **32**, 2198 (1961).

[31] U. Birkholz, Naturforsch. **13a**, 780 (1958).

[32] F. D. Rosi, B. Abeles, and R. V. Jensen, J. Phys. Chem. Solids **10**, 191 (1959).

[33] K. Yokota and S. Katayama, Jpn. J. Appl. Phys. **12**, 1205 (1973).

[34] C. B. Satterthwaite and J. R. W. Ure, Phys. Rev. **108**, 1164 (1957).

[35] R. A. Ismaiylova, I. B. Bakhtiyarly, and D. Sh. Abdinov, Inorg. Mater. **45**, 744 (2009).

[36] M. Stordeur and G. Simon, Phys. Status Solidi B **124**, 799 (1984).

[37] J. S. Dyck, W. Chen, C. Uher, Č. Drašar, and P. Lošt'ák, Phys. Rev. B **66**, 125206 (2002).

[38] Č. Drašar, M. Steinhart, P. Lošt'ák, H.-K. Shin, J. S. Dyck, and C. Uher, J. Solid State Chem. **178**, 1301 (2005).

[39] F. Yang, T. Ikeda, G. J. Snyder, and C. Dames, J. Appl. Phys. **108**, 034310 (2010).

[40] W. M. Yim and F. D. Rosi, Solid State Electron **15**, 1121 (1972).

[41] L.-D. Zhao, B.-P. Zhang, J.-F. Li, M. Zhou, W.-S. Liu, and J. Liu, J. Alloys Compd. **455**, 259 (2008).

[42] D. Stroud, Phys. Rev. B **12**, 3368 (1975).